

Rapid Crypt Cell Remodeling Regenerates the Intestinal Stem Cell Niche after Notch Inhibition

Natacha Bohin,^{1,2,7} Theresa M. Keeley,^{1,7} Alexis J. Carulli,¹ Emily M. Walker,¹ Elizabeth A. Carlson,¹ Jie Gao,⁴ Iannis Aifantis,⁴ Christian W. Siebel,⁵ Michael W. Rajala,³ Martin G. Myers, Jr.,^{1,2,3} Jennifer C. Jones,⁶ Constance D. Brindley,⁶ Peter J. Dempsey,⁶ and Linda C. Samuelson^{1,2,3,*}

¹Department of Molecular & Integrative Physiology, University of Michigan, Ann Arbor, MI 48109, USA

²Program in Cellular and Molecular Biology, University of Michigan, Ann Arbor, MI 48109, USA

³Department of Internal Medicine, University of Michigan, Ann Arbor, MI 48109, USA

⁴Department of Pathology, New York University School of Medicine, New York, NY 10016, USA

⁵Department of Discovery Oncology, Genentech, Inc, South San Francisco, CA 94080, USA

⁶Department of Pediatrics, University of Colorado Medical School, Aurora, CO 80045, USA

⁷Co-first author

*Correspondence: lcsam@umich.edu

<https://doi.org/10.1016/j.stemcr.2020.05.010>

SUMMARY

Intestinal crypts have great capacity for repair and regeneration after intestinal stem cell (ISC) injury. Here, we define the cellular remodeling process resulting from ISC niche interruption by transient Notch pathway inhibition in adult mice. Although ISCs were retained, lineage tracing demonstrated a marked reduction in ISC function after Notch disruption. Surprisingly, Notch ligand-expressing Paneth cells were rapidly lost by apoptotic cell death. The ISC-Paneth cell changes were followed by a regenerative response, characterized by expansion of cells expressing Notch ligands *Dll1* and *Dll4*, enhanced Notch signaling, and a proliferative surge. Lineage tracing and organoid studies showed that *Dll1*-expressing cells were activated to function as multipotential progenitors, generating both absorptive and secretory cells and replenishing the vacant Paneth cell pool. Our analysis uncovered a dynamic, multicellular remodeling response to acute Notch inhibition to repair the niche and restore homeostasis. Notably, this crypt regenerative response did not require ISC loss.

INTRODUCTION

As one of the most rapidly renewing tissues, the intestine has a great capacity for regeneration. Under homeostatic conditions, *Lgr5*+ crypt base columnar stem cells (CBCs) are responsible for replenishing the intestinal epithelium throughout life (Barker et al., 2007). This intestinal stem cell (ISC) population generates highly proliferative transit amplifying progenitors which differentiate into various mature epithelial cell types. Most newly formed differentiated cells move out of the crypts and onto the villi, where they function in absorption or secretion before being extruded into the lumen, with a half-life of several days. The exception is Paneth cells, which move to the crypt base to lie adjacent to CBCs, with a half-life of several weeks (Ireland et al., 2005).

When CBCs are lost, other crypt cell populations can replace their function, acting as facultative stem cells ([FSCs] also called +4 cells, reserve stem cells, or quiescent stem cells) by reentering the cell cycle to generate progeny that can maintain the epithelium during the repair process and to occupy vacant stem cell niche spaces to replace lost CBCs (Bankaitis et al., 2018). FSC activation after intestinal injury has been demonstrated by lineage tracing from several different Cre drivers that mark various lineage-committed (*Alpi*, *Dll1*) or slowly cycling (*Bmi1*, *Hopx*, *Lrig1*, *mTert*) crypt progenitor

cell populations (Montgomery et al., 2011; Powell et al., 2012; Roth et al., 2012; Sangiorgi and Capecchi, 2008; Takeda et al., 2011; Tetteh et al., 2016; Tian et al., 2011; van Es et al., 2012; Yan et al., 2012), as well as differentiated Paneth (*Defa4*, *Lyz1*) or endocrine (*NeuroD1*) cells (Jones et al., 2019; Sei et al., 2018; Yu et al., 2018). Thus, in response to stem cell injury, numerous cell populations in the intestinal crypt exhibit remarkable cellular plasticity to reprogram their cell fate and function like stem cells to regenerate the crypt and return to homeostasis.

Adult stem cells are regulated by their niche, the tissue-specific microenvironment of cells, secreted substances, and extracellular matrix that provide key signaling factors to orchestrate stem cell function. In the intestine, the stem cell niche includes both epithelial and stromal cell compartments (Santos et al., 2018). Wnt/R-spondin and Notch signaling have been identified as the primary niche pathways promoting ISC self-renewal, with pathway disruption leading to CBC loss and crypt collapse. While ISC Wnt signaling is regulated by ligands secreted from both epithelial and stromal cell sources (Degirmenci et al., 2018; Farin et al., 2012; Greicius et al., 2018; San Roman et al., 2014; Shoshkes-Carmel et al., 2018), Notch signaling in the crypt is likely to be epithelial specific because it requires direct cell-to-cell contact (Dempsey et al., 2018).





CBCs have been demonstrated to be Notch-signaling cells (Fre et al., 2005; Pellegrinet et al., 2011; VanDussen et al., 2012), with Notch1 identified as the primary receptor regulating CBC function (Carulli et al., 2015). Notch inhibition results in CBC loss and expansion of secretory cell types, including goblet, endocrine, and Paneth-like cells (Pellegrinet et al., 2011; Riccio et al., 2008; van Es et al., 2005; VanDussen et al., 2012). Interestingly, the Paneth-like cells have altered secretory granule morphology and co-express Paneth and goblet cell markers, suggesting that Paneth cells are particularly sensitive to Notch perturbation although they are not Notch signaling cells (VanDussen et al., 2012). Paneth cells are the most likely source of Notch ligand due to their close association with CBCs at the crypt base (Sato et al., 2011). Moreover, Paneth cells express both *Dll1* and *Dll4* (Sasaki et al., 2016; Sato et al., 2011), the key Notch ligands regulating CBC function (Pellegrinet et al., 2011).

In spite of our understanding of CBC niche regulation during homeostasis, little is known about niche responses after injury. Earlier studies of genetic Notch disruption or pharmacologic Notch inhibition via administration of a gamma-secretase inhibitor (GSI) such as dibenzazepine (DBZ), were limited by the reduced animal viability observed when inhibition extended over several days, which impeded analysis of the regeneration process. Indeed, the intestinal toxicity imparted by Notch inhibitors limits use in the clinic despite their great therapeutic potential for treating Notch-driven cancers (e.g., T cell acute lymphoblastic leukemia) and other diseases. Short-term Notch inhibition may be one approach to maintain ISCs and minimize toxicity in human patients, yet there is little known about ISC responses to short-term Notch interruption. Here, we introduce an intestinal crypt disruption model based on short-term niche factor inhibition. We probe the setting of pharmacologic inhibition to investigate the acute cellular response to Notch niche disruption. We demonstrate that short-term Notch disruption leads to transient ISC dysfunction and dynamic crypt cell remodeling. This process is highlighted by rapid Paneth cell loss, a novel contrast to previous findings established by studies using longer time points of Notch inhibition that demonstrated Paneth-like cell expansion. Furthermore, after short-term Notch disruption we observed an expansion of cells expressing Notch ligands and increased Notch signaling, with a regenerative response characterized by a proliferative surge. We show that *Dll1*⁺ cells are activated to function as multipotential progenitors to maintain the epithelium during ISC dysfunction, including replenishment of the vacant Paneth cell population. Our study sheds light into how niche pathways and crypt cell plasticity orchestrate intestinal repair.

RESULTS

Impaired CBC Function after Acute Notch Inhibition

We analyzed the immediate effect of Notch inhibition on ISC function and characterized the crypt regenerative response after short-term pathway disruption in adult mice treated with a single dose of DBZ. Intestinal tissue was isolated at various times post-DBZ, which has a plasma half-life of less than 12 h (Milano et al., 2004), to characterize the dynamic crypt cell response (Figure 1A). We observed rapid loss of expression of the CBC marker (van der Flier et al., 2009) and Notch target gene (VanDussen et al., 2012) *Olfm4* as early as 12 h post-DBZ, with expression returning at day 3 (Figures 1B, 1C, and S1A). In contrast, expression of the CBC Wnt target gene *Lgr5* was not changed (Figures 1B and 1C), suggesting that the dynamic changes to *Olfm4* reflected loss of CBC Notch signaling rather than stem cell depletion.

To assess the effect of acute Notch inhibition on CBC function, we measured lineage tracing using two different CBC-specific Cre driver strains (*Olfm4-GFP-CreER^{T2}* and *Lgr5-GFP-CreER^{T2}*) crossed to the *ROSA26-LSL-tdTomato* (Tom) reporter. The Tom lineage mark was activated in CBCs by treatment with tamoxifen (TX), followed by DBZ or vehicle (Veh) treatment, with analysis 1 day later (Figure 1D). We observed significantly fewer lineage-traced cells in DBZ-treated mice compared with Veh-treated controls (Figure 1E). Quantification of the number of Tom-labeled cells per crypt showed that DBZ-treated *Olfm4* and *Lgr5* reporter mice had an approximately 2-fold reduction in lineage tracing, demonstrating impaired CBC function (Figure 1E). Interestingly, the Tom-labeled cells were clustered at the crypt base in a pattern distinct from the Veh-treated controls, suggesting crypt cell remodeling post-DBZ (Figure 1E).

Rapid Paneth Cell Apoptosis after Acute Notch Inhibition

Histological analysis of the crypt post-DBZ showed dynamic cellular remodeling. Remarkably, granule-filled Paneth cells at the crypt base were lost within 12 h of DBZ administration, together with the appearance of delaminated cells (Figure 2A, arrowheads). To further examine this effect, we analyzed the expression of Paneth cell-specific markers by immunostaining (lysozyme) and qRT-PCR (cryptdins), showing that both were markedly reduced in DBZ-treated crypts as early as 12 h after administration (Figures 2B and 2C). To determine whether the loss of Paneth cell marker expression was due to cellular remodeling or cell loss, we used *Defensin α 4-Cre;Tom* mice, which permanently label Paneth cells with a Tom lineage mark. We observed a marked loss of Tom-labeled cells 1 day

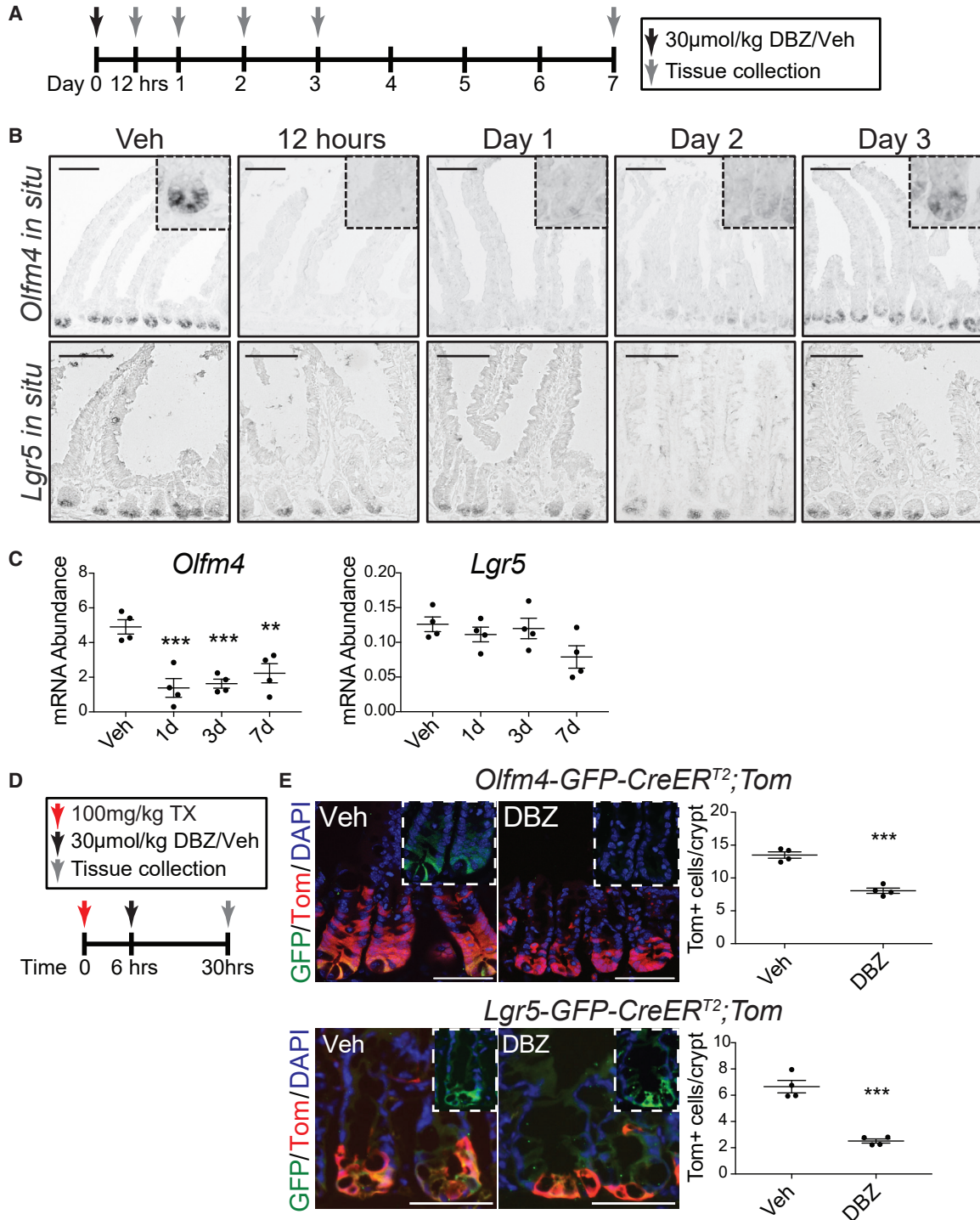


Figure 1. Impaired CBC Function after Acute Notch Inhibition

(A) Mice were treated with dibenzazepine (DBZ) (30 μmol/kg) or vehicle (Veh) and duodenal tissue was collected at various times.
 (B) *In situ* hybridization for crypt base columnar (CBC) stem cell markers *Olfm4* and *Lgr5*. Insets are 3× original magnification. Scale bars, 100 μm.
 (C) qRT-PCR analysis of mRNA abundance relative to *Hprt*. Quantitative data are presented as mean ± SEM (**p = 0.0037, ***p < 0.001, Veh versus DBZ by one-way ANOVA with Dunnett's post-test; n = 4 mice/group).
 (D) Stem cell function was measured by lineage tracing after tamoxifen (TX) activation and DBZ or Veh treatment, as shown.
 (legend continued on next page)



post-DBZ in these mice, confirming that Notch inhibition led to rapid Paneth cell loss (Figure 2B, insets). Analysis of apoptosis by staining for cleaved caspase-3 showed a significant increase in apoptotic cells in the crypts, which peaked at 1 day post-DBZ (Figure 2D). Co-staining for the Paneth cell marker MMP7 and cleaved caspase-3 showed that the apoptotic cells were Paneth cells (Figure 2E).

Our findings suggest that Notch signaling is required for Paneth cell maintenance, which is unexpected as Paneth cells do not express Notch receptors or exhibit Notch signaling. To confirm that Paneth cell loss is a consequence of Notch inhibition and not due to the inhibition of another GSI target, we analyzed *Defensin α 4-Cre;Tom* mice that were treated with a mixture of inhibitory antibodies to DLL1 and DLL4, the two Notch ligands required for crypt homeostasis (Pellegrinet et al., 2011). Similar to our findings after DBZ treatment, we observed reduced Paneth cell numbers after combined DLL1 and DLL4 Notch-signaling blockade, showing that Paneth cell loss is due to Notch inhibition (Figure S1). Paneth cell loss may explain reduced CBC function, shown by loss of *Olfm4* and diminished lineage tracing post-DBZ (Figure 1), as Paneth cells are known to express several ISC niche factors (Sato et al., 2011). Notably, Paneth cells are returning by 3 days after acute Notch inhibition, with an apparent increase in numbers of granule-containing cells and Tom-marked cells by day 7, suggesting a rebound effect (Figures 2A and 2B). Interestingly, Paneth cells returning at day 3 corresponds to the timing of return of expression of *Olfm4* (Figure 1B). The coincident reemergence of *Olfm4* expression with Paneth cells was confirmed by co-imaging lysozyme and GFP in DBZ-treated *Olfm4-GFP-CreER^{T2}* intestine, with GFP expression detected in stem cells adjacent to lysozyme-expressing Paneth cells (Figure 2F).

Increased Notch Activity and Cell Proliferation during Crypt Regeneration

We assessed proliferation after DBZ treatment to determine if crypt remodeling included a regenerative response. Acute Notch inhibition resulted in a marked increase in proliferation at day 3, with a 1.6-fold increase in 5-ethynyl-2'-deoxyuridine (EdU+) cells (Figures 3A and 3B). This proliferative surge was accompanied by dynamic changes in crypt cellularity. Decreased crypt cellularity was observed at 1 day post-DBZ (Figure 3C), a time point marked by loss of Paneth cells and diminished CBC stem cell function. However, at the time of the proliferative surge at day 3,

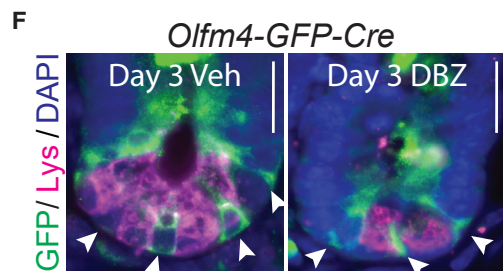
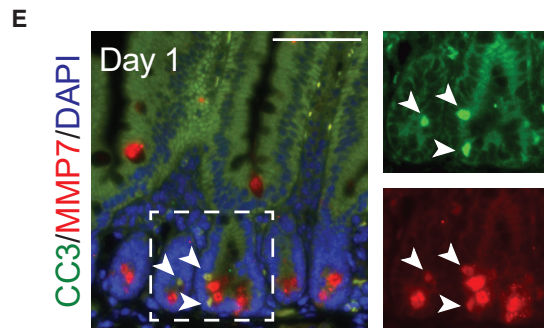
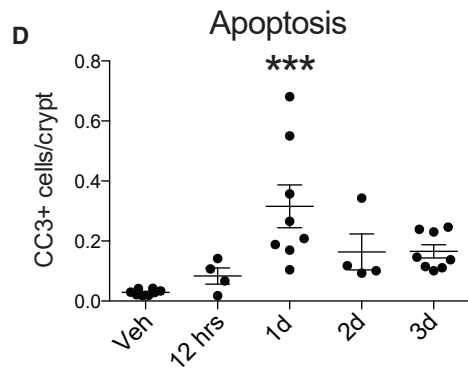
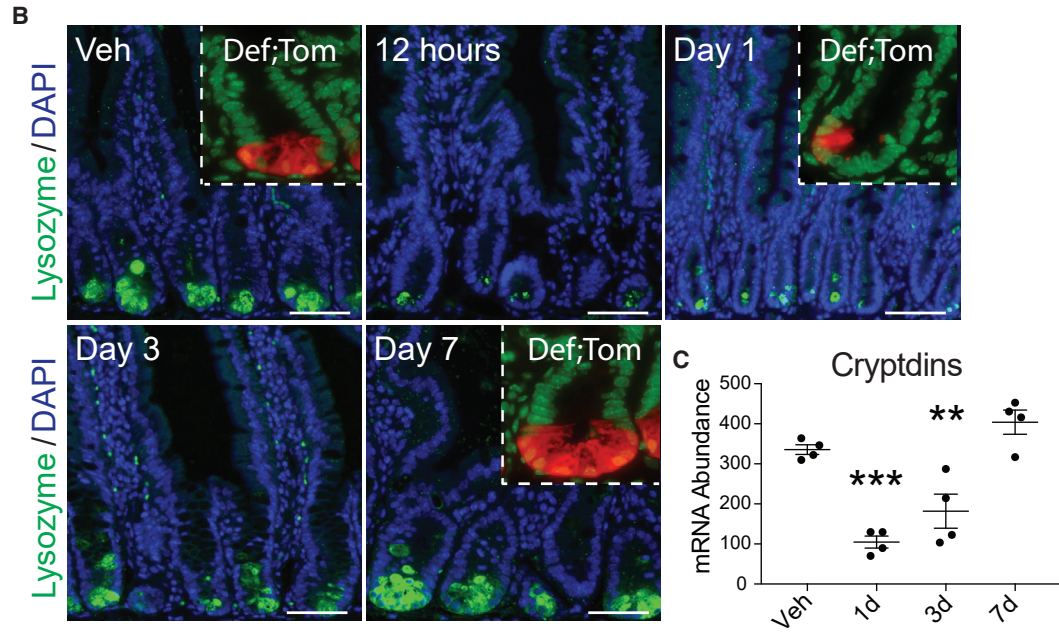
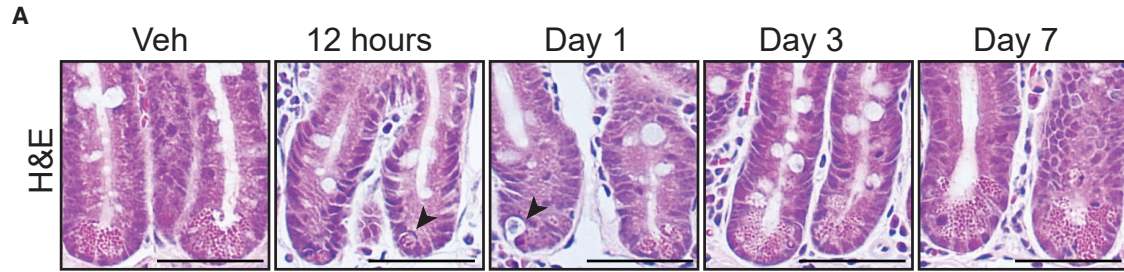
crypts were expanded with increased cellularity compared with Veh-treated mice (Figures 3A and 3C).

Given the well-characterized role of Notch signaling to regulate intestinal proliferation (Fre et al., 2005; Pellegrinet et al., 2011; Riccio et al., 2008; Stanger et al., 2005; van Es et al., 2005; VanDussen et al., 2012), we investigated Notch activity to determine if the hyperproliferative response coincided with the return of Notch function. Immunostaining for the NOTCH1 intracellular signaling domain (NICD) showed loss of Notch activity 12 h post-DBZ (Figures 3D and 3E), which is consistent with the loss of expression of the Notch target gene *Olfm4* at that time point (Figure 1B). NICD+ cell numbers increased over time, and by day 3 the number of NICD+ cells was markedly increased in comparison with Veh control, which coincided with the timing of increased proliferation and crypt cellularity. Interestingly, co-staining for NICD and EdU showed that proliferating cells at day 3 post-DBZ were commonly Notch-signaling cells, while most EdU+ cells in Veh control were NICD⁻ (Figure 3F). Furthermore, NICD+ cells were preferentially localized in the mid-crypt region when they are returning, in contrast to their normal localization at the crypt base. Occasional cells at the crypt base are NICD+ at day 3, in accordance with the timing of the return of Paneth cells and *Olfm4* expression (Figure 3D, arrowheads).

Rapid Expansion of Dll1- and Dll4-Expressing Cells during Crypt Regeneration

The rebounding Notch activity after acute Notch inhibition is associated with increased mRNA abundance of key Notch components, including ligands *Dll1* and *Dll4* (Pellegrinet et al., 2011), and receptors *Notch1* and *Notch2* (Carulli et al., 2015; Riccio et al., 2008) (Figure 4A). We made use of *Dll1-mCherry* and *Dll4-mCherry* transgenic reporter mice (Chakrabarti et al., 2018; Tikhonova et al., 2019) to follow the cellular pattern of Notch ligand-expressing cells during intestinal remodeling post-DBZ. Analysis of these reporter mice showed that *Dll1-* and *Dll4-mCherry+* cells are normally present in both intestinal crypt and villus compartments in a scattered pattern consistent with secretory cell distribution (Figure 4B). We identified the cell types by co-imaging *mCherry* with markers of differentiated Paneth (lysozyme), goblet (mucin 2), and endocrine (chromogranin A) cells. This analysis showed that all three secretory cell types are marked with the mCherry reporter in both transgenic strains (Figure S2). This cellular expression pattern matches that previously characterized in

(E) Tomato (Tom) lineage stripes were measured in *Olfm4-GFP-CreER^{T2};ROSA26-LSL-tdTomato (Tom)* (top) or *Lgr5-GFP-CreER^{T2};Tom* (bottom) duodenum. Insets show green channel to image CBCs. Quantification of the number of Tom+ cells per crypt in Veh- and DBZ-treated mice. Scale bars, 50 μ m. Quantitative data are presented as mean \pm SEM (***) $p < 0.001$, Veh versus DBZ by Student's *t* test; $n = 4$ mice/group). 30–50 crypts per mouse were counted.



(legend on next page)



Dll1-GFP-CreER^{T2} mice, with GFP expression observed in differentiated secretory cell types as well as secretory progenitor cells (van Es et al., 2012). The cellular expression pattern was similar in DBZ-treated *Dll1*- and *Dll4-mCherry* mice, with the exception of the Paneth cell loss (Figure S2).

Numbers of *Dll1*- and *Dll4-mCherry*⁺ cells were markedly increased after Notch inhibition, accounting for increased mRNA abundance (Figure 4B). Notch ligand-expressing cell expansion corresponds to a surge in goblet cell numbers detected by PAS/Alcian blue staining (Figure S3). This finding is consistent with previous reports of secretory cell hyperplasia after several days of continuous Notch inhibition (van Es et al., 2005; VanDussen et al., 2012). *Dll1*- and *Dll4-mCherry*⁺ cell expansion was profound, with expanded crypts at day 3 extensively composed of Notch ligand-expressing cells (Figure 4B). Quantification of *Dll1-mCherry*⁺ cells by flow cytometry showed that cell number increased 2.6-fold at 1 day post-DBZ (Figure 4C), with ligand-expressing cells primarily located at the crypt base (Figure 4B).

Increased Progenitor Cell Function in *Dll1*-Expressing Cells after Acute Notch Inhibition

Interestingly, both *Dll1-mCherry*⁺ cells and *Lgr5*-expressing CBCs were localized to the crypt base 1 day post-DBZ (Figures 1 and 4), suggesting that CBCs might activate *Dll1* expression in response to Notch inhibition. To examine this possibility, we treated *Lgr5-GFP-CreER^{T2};Dll1-mCherry* mice with DBZ, and co-imaged GFP and mCherry by histological and fluorescence-activated cell sorting (FACS) analysis. This work identified GFP⁺/mCherry⁺ co-expressing cells at the crypt base, suggesting that *Lgr5* CBCs turn on *Dll1* after Notch niche inhibition (Figures 5A and S4). Furthermore, we observed increased proliferation of *Dll1*⁺ cells 1 day post-DBZ, showing a 5-fold increase in EdU⁺/mCherry⁺ double-positive cells compared with Veh control (Figures 5B and 5C). We next tested whether *Dll1-mCherry*⁺ cells had increased stem/progenitor cell function

by measuring organoid-forming potential of single *Dll1-mCherry*⁺ cells isolated by flow cytometry 1 day post-DBZ. This analysis showed a 2-fold increase in organoid-forming efficiency compared with *Dll1-mCherry*⁺ cells isolated from Veh-treated mice (Figure 5D). Together these findings suggest that *Dll1*⁺ cells exhibit enhanced progenitor cell status 1 day post-DBZ.

Multiple Progenitor Cell Populations Generate Paneth Cells after Acute Notch Inhibition

We next studied whether FSCs are activated by Notch niche interruption to maintain the epithelium and replenish the lost Paneth cell population. In particular, we focused on *Dll1*-expressing secretory progenitors as this crypt cell population was previously demonstrated to regenerate CBCs after irradiation-induced crypt injury (van Es et al., 2012). We used a lineage-tracing approach in *Dll1-GFP-CreER^{T2};Tom* mice (Figure 6A). Note that this analysis differs from our studies above in that Tom marks cells prior to DBZ treatment, thus allowing us to study pre-existing *Dll1*⁺ cells rather than the new cells that emerge after Notch inhibition. At 8 days after TX treatment, the only Tom⁺ cells in Veh controls were Paneth cells, due to their long half-life; all other Tom⁺ cells had turned over by this time (Figure 6B). In contrast, DBZ-treated crypts contained numerous Tom⁺ cells, including lineage stripes (Figure 6B, inset). Quantification showed that DBZ-treated mice commonly exhibited lineage stripes, while Veh-treated mice exhibited none (Figure 6C). We determined which cell types were generated by the activated *Dll1*⁺ cells by staining for markers of absorptive (enterocytes) and secretory (goblet, endocrine, Paneth) cells with Tom co-expression (Figure 6D). This analysis showed that DBZ-activated *Dll1*⁺ cells become multipotential progenitors, capable of generating all of the major epithelial cell types. Thus, they function to maintain the intestinal epithelium while CBCs are impaired.

Figure 2. Rapid Paneth Cell Apoptosis after Acute Notch Inhibition

(A) Mice were treated with DBZ or Veh and duodenal tissue was analyzed by H&E staining. Arrowheads denote delaminated cells.
 (B) Duodenal tissue sections were immunostained for the Paneth cell marker lysozyme (green), with nuclear DAPI (blue). Insets depict ileal crypts from *Defensin α4-Cre;Tom* (Def; Tom) mice with Tom-marked Paneth cells (red), with DAPI (green). Scale bars, 50 μm.
 (C) qRT-PCR analysis of Paneth cell cryptdins mRNA abundance relative to *Hprt*. Quantitative data are presented as mean ± SEM (**p = 0.0055, ***p = 0.0002, Veh versus DBZ by one-way ANOVA and Dunnett's post-test; n = 4 mice/group).
 (D and E) Apoptotic cells were detected by immunostaining for cleaved caspase-3 (CC3) (green), (D) quantified in the duodenum at various time points after Veh or DBZ, and (E) co-stained with the Paneth cell marker MMP7 (red) with DAPI (blue). Single green and red channel images for the inset are shown on the right. Arrowheads denote co-stained cells. Scale bar, 50 μm. Quantitative data are presented as mean ± SEM (***p = 0.0001, Veh versus DBZ by one-way ANOVA and Dunnett's post-test; n = 4–8 mice/group, as shown). Approximately 150 crypts per mouse were counted.
 (F) Duodenal crypts from *Olfm4-GFP-CreER^{T2}* mice were stained for GFP (green) and lysozyme (Lys, magenta) at day 3 post-Veh or DBZ to image *Olfm4*⁺ CBCs (arrowheads) and Paneth cells. Scale bars, 10 μm.
 See also Figure S1.

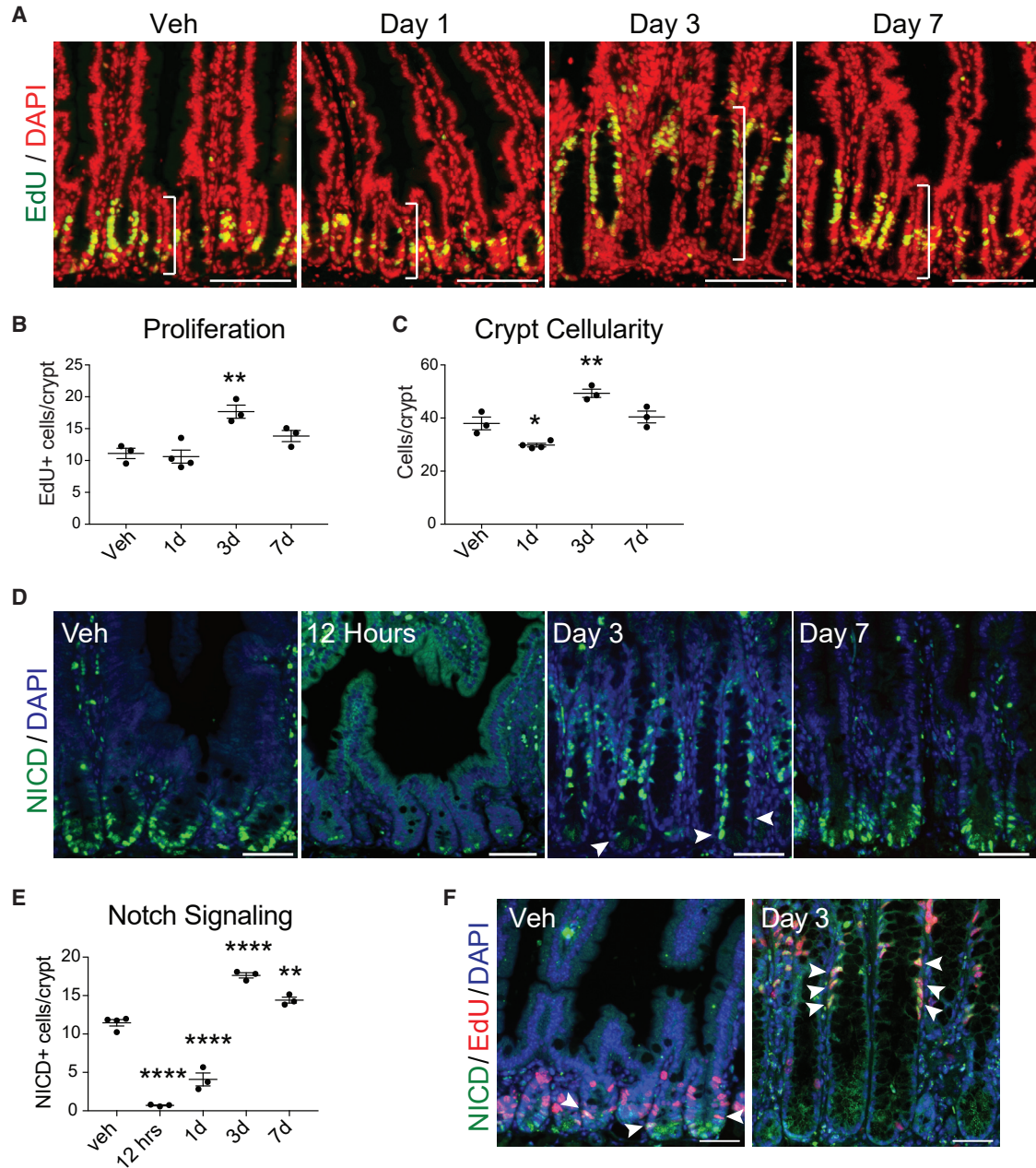


Figure 3. Increased Notch Activity and Cell Proliferation during Crypt Regeneration

(A) Cellular proliferation was assessed in Veh- and DBZ-treated mouse duodenum at various timepoints by EdU incorporation (green) with DAPI (red). White brackets mark crypt depth. Scale bars, 100 μ m.

(B) Quantification of EdU+ cells per crypt. Quantitative data are presented as mean \pm SEM (** p = 0.0034, Veh versus DBZ by one-way ANOVA and Dunnett's post-test; n = 3–4 mice/group, as shown). Approximately 30 crypts were counted per mouse.

(C) Crypt cellularity was determined by counting DAPI+ nuclei per crypt. Quantitative data are presented as mean \pm SEM (* p = 0.0166, ** p = 0.0035, Veh versus DBZ by one-way ANOVA and Dunnett's post-test; n = 3–4 mice/group, as shown). Approximately 30 crypts were counted per mouse.

(D) Notch signaling at various times post-DBZ treatment was measured by immunostaining duodenal tissue sections for the NOTCH1 intracellular domain NICD (green) with DAPI (blue). Arrowheads indicate NICD+ cells at the crypt base at day 3. Scale bars, 50 μ m.

(legend continued on next page)



Importantly, we found that the Tom⁺ cells generated from activated *Dll1*⁺ multipotential progenitors included Paneth cells (Figure 6D). Quantification of lysozyme/Tom double-positive cells showed increased numbers of lineage-labeled Paneth cells in DBZ-treated crypts compared with Veh control (Figure 6E). In light of the DBZ-induced Paneth cell loss (Figure 2), the observation of numerous Tom⁺ Paneth cells demonstrates that activated *Dll1*⁺ multipotential progenitors are replenishing the depleted Paneth cell pool.

The observation that *Dll1*⁺ cells contributed to differentiated cell lineages after acute Notch inhibition is consistent with FSC activity. However, lineage stripes from *Dll1*⁺ cells were short lived, with no lineage traces detected at 2 months post-DBZ (Figures 6C and 6F). Thus, these activated multipotential progenitors do not contribute to the CBC pool. This result is in agreement with our finding that CBCs are not lost after DBZ treatment (Figure 1). Further evidence that CBCs were maintained after DBZ was shown by the resumption of CBC lineage tracing in *Lgr5-GFP-CreER^{T2};Tom* mice, with full crypt-villus Tom-labeling observed 7 days post-DBZ treatment (Figures 6G and 6H). Thus, CBC function was only transiently impaired after DBZ treatment. The data suggest that DBZ treatment activates *Dll1*⁺ cells to become multipotential progenitors to contribute to crypt regeneration after injury induced by Notch inhibition but not to displace resident CBCs.

Notably, we also observed Tom⁺ Paneth cells in *Lgr5-GFP-CreER^{T2};Tom* mice (Figure 6H, inset, arrowhead). Together with the *Dll1*⁺ cell lineage-tracing data, this shows that multiple stem/progenitor cell populations can replenish the depleted Paneth cell pool. To test if other progenitor cell populations capable of FSC activity were activated after acute DBZ treatment, we carried out lineage-tracing studies in *Hopx-CreER^{T2};ROSA26-LSL-mTmG* mice. In contrast to our result with *Dll1*⁺ cells, we did not observe enhanced lineage tracing from *Hopx*⁺ cells after DBZ treatment (Figure S5). This result suggests that the damage induced by Notch inhibition activates specific progenitor populations to contribute to the crypt repair process.

DISCUSSION

Our study uncovered a rapid and dynamic crypt cell remodeling program stimulated by interruption of the ISC Notch

niche. We revealed that transient Notch inhibition induces a multicellular remodeling response, highlighted by a striking, early Paneth cell loss via apoptotic cell death. Although CBC stem cells are retained, they exhibit a transient impairment in function, characterized by loss of lineage-tracing activity coincident with disappearance of Notch signaling. A regenerative response followed the Paneth cell-CBC stem cell disruption, with repair and return to homeostasis within a few days. The repair involves expansion of Notch ligand-expressing cells, followed by concurrent surges in Notch signaling and cell proliferation. *Dll1*⁺ cells were activated to proliferate and function as multipotential progenitors to generate new epithelial cells, including absorptive enterocytes as well as secretory cell types. Thus these cells essentially adopt stem cell-like function to transiently maintain the epithelium and contribute to the replenishment of the depleted Paneth cell pool. This dynamic multicellular remodeling response to acute Notch inhibition is summarized in Figure 7.

Our findings differ in many respects from previous studies of Notch inhibition, which analyzed longer-lasting pharmacologic (Tian et al., 2015; van Es et al., 2005; VanDussen et al., 2012) or genetic (Carulli et al., 2015; Pellegrinet et al., 2011; Tsai et al., 2014) Notch depletion. In these earlier studies, long-lasting Notch inhibition led to CBC loss and a marked decrease in crypt proliferation, together with a surge of secretory cell types. Thus, our observation of *Lgr5*⁺ CBC stem cell retention and increased proliferation after short-term Notch disruption were unexpected. There is general agreement, however, that continuous Notch signaling is required to maintain CBC stem cells, with pathway interruption leading to rapid stem cell dysfunction and ultimately cell loss, depending on the duration of pathway inhibition.

Our observation of rapid Paneth cell death was in stark contrast to the robust expansion of lysozyme-expressing cells seen in long-term Notch inhibition studies. However, these were not “true” Paneth cells as they exhibited altered secretory granule morphology and co-expressed goblet cell markers (VanDussen et al., 2012). Interestingly, Paneth cell loss was also observed in a distinct study of CBC niche disruption that blocked R-spondin signaling in CBCs using an adenoviral construct that targeted LGR5 (Yan et al., 2017). However, Paneth cell loss with this niche disruptor was considerably slower, involving a process of ballooning cellular degeneration and upward migration that took several days, instead of the rapid

(E) Quantification of NICD⁺ cells per duodenal crypt after Veh or DBZ. Quantitative data are presented as mean ± SEM (**p < 0.0028, ****p < 0.0001 Veh versus DBZ by one-way ANOVA and Dunnett's post-test; n = 3–4 mice/group, as shown). Approximately 50 crypts per mouse were counted.

(F) Correspondence of Notch signaling with cellular proliferation was determined at day 3 post-Veh or -DBZ by immunostaining for NICD (green) and Edu (red), with DAPI (blue). Arrowheads indicate co-stained cells. Scale bars, 50 μm.

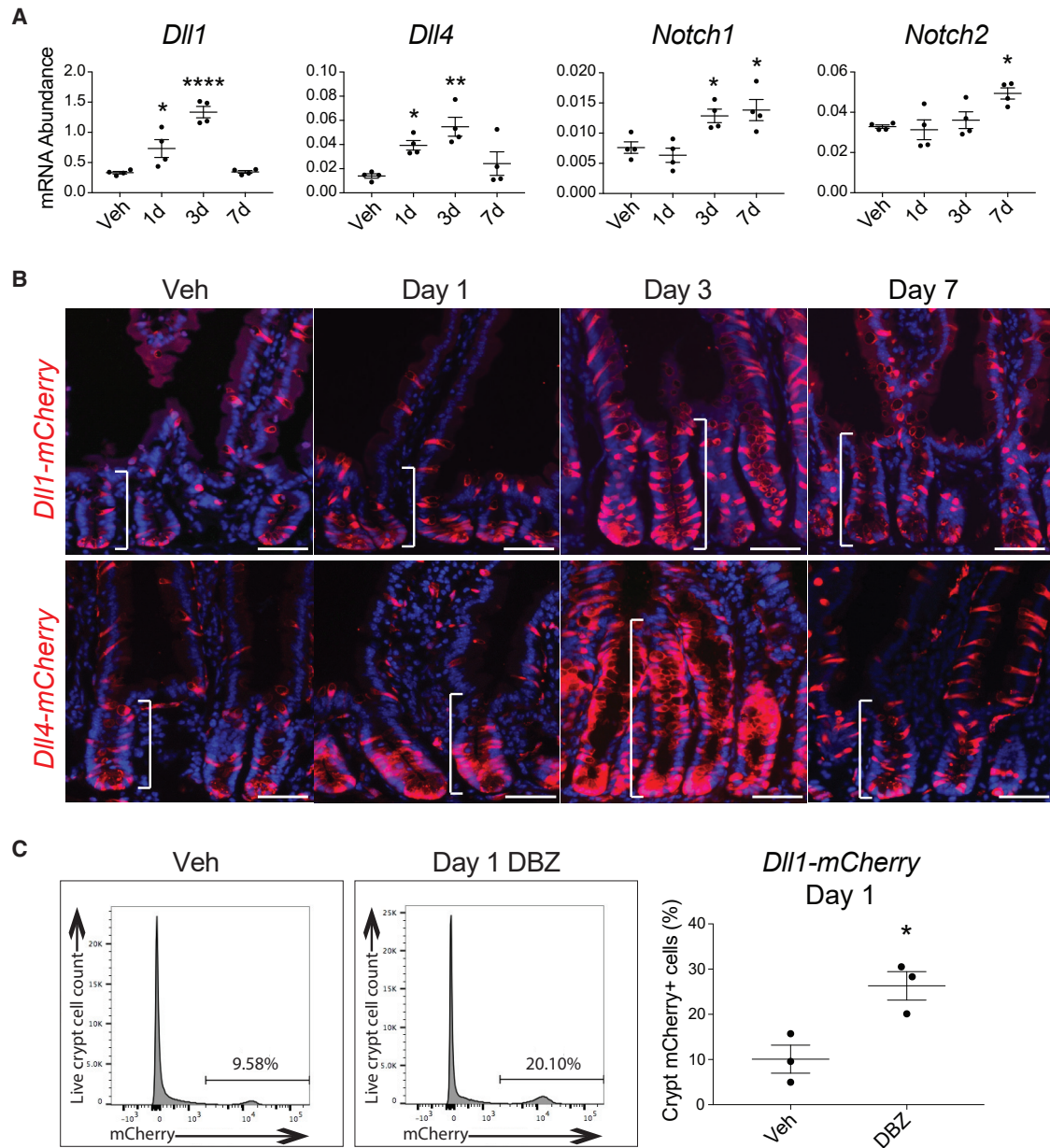


Figure 4. Rapid Expansion of *Dll1*- and *Dll4*-Expressing Cells during Crypt Regeneration

(A) qRT-PCR analysis of mRNA abundance of key Notch ligands and receptors in Veh- and DBZ-treated mouse duodenal crypts relative to *Hprt*. Quantitative data are presented as mean \pm SEM (* p < 0.05, ** p < 0.01, **** p < 0.0001, Veh versus DBZ by one-way ANOVA and Dunnett's post-test; n = 3–4 mice/group, as shown).

(B) *Dll1-mCherry* and *Dll4-mCherry* transgenic mice were treated with Veh or DBZ and mCherry+ cells (red) were imaged in duodenal sections with DAPI (blue). White brackets mark crypt depth. Scale bars, 50 μ m.

(C) Flow cytometric quantification of the number of mCherry+ cells in *Dll1-mCherry* duodenal crypts 1 day post-Veh or -DBZ. Quantitative data are presented as mean \pm SEM (* p = 0.0216, Veh versus DBZ by Student's t test; n = 3 mice/group).

See also Figures S2 and S3.

apoptotic cell death we observed with Notch niche inhibition. Together, our study and the Yan et al. study demonstrate that Paneth cells are very sensitive to CBC niche dysfunction, including both Notch and R-spondin

pathway inhibition. The findings suggest that CBC niche disruption affects Paneth cell maintenance through an indirect mechanism as both studies targeted receptors specifically localized to CBCs.

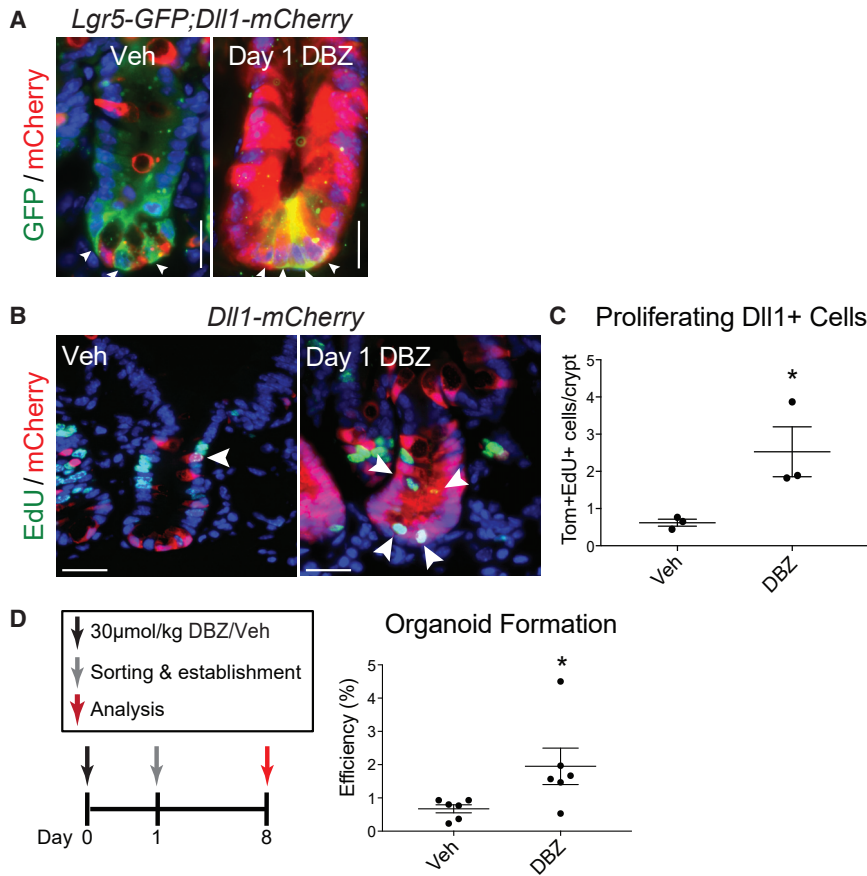


Figure 5. Increased Progenitor Cell Function in *Dll1*-Expressing Cells after acute Notch Inhibition

(A) *Lgr5-GFP-CreERT²;Dll1-mCherry* mice were imaged for *Lgr5-GFP* (green) and *mCherry* (red) 1 day post-Veh or -DBZ. Arrowheads point to *Lgr5-GFP*+/*mCherry*+ CBCs. Scale bars, 20 µm.

(B) *Dll1-mCherry* mice were treated with Veh or DBZ and proliferation was measured 1 day later by EdU incorporation. Arrowheads highlight *mCherry* (red) and EdU (green) co-stained cells, which represent proliferating *Dll1*+ progenitors. Scale bars, 25 µm.

(C) The number of proliferating *Dll1-mCherry* cells per duodenal crypt was quantified. Quantitative data are presented as mean ± SEM (**p* = 0.0481, Veh versus DBZ by Student's *t* test; *n* = 3 mice/group). Approximately 30 crypts per mouse were counted.

(D) Schematic of organoid formation assay used to measure stem cell-like activity of *mCherry*+ cells isolated by FACS from *Dll1-mCherry* mice 1 day after Veh or DBZ. Organoid-forming efficiency is presented as percent of the number of cells plated that formed organoids. Quantitative data are presented as mean ± SEM (**p* = 0.0457, Veh versus DBZ by Student's *t* test; *n* = 6 mice/group with three technical replicates per mouse).

See also Figure S4.

Paneth cells have been proposed to be Notch niche cells due to their close physical association with CBCs at the crypt base and their expression of *Dll1* and *Dll4*, the key Notch ligands regulating CBC function (Pellegrinet et al., 2011; Sasaki et al., 2016; Sato et al., 2011). In addition, Paneth cells generate other niche factors, including Wnt ligands and growth factors, as well as metabolic products, suggesting a more expanded niche role for Paneth cells to support their stem cell neighbors (Rodriguez-Colman et al., 2017; Sato et al., 2011). However, niche function for Paneth cells has been controversial, with some studies showing that Paneth cells enhance stem cell function (Farin et al., 2012; Sato et al., 2011), while others demonstrate apparently normal CBC function after Paneth cell depletion (Durand et al., 2012; Garabedian et al., 1997; Kim et al., 2012; van Es et al., 2019). Our observation of reduced CBC lineage-tracing activity with Paneth cell loss, and a return to stem cell function with Paneth cell return, would support a functional niche role for Paneth cells. Notably, Notch signaling and *Olfm4* expression at the crypt base did not recover until Paneth cells were restored at day 3, suggesting that Paneth cells are the key Notch niche cells presenting ligand to CBCs. Interestingly,

we observed that *Lgr5* CBCs activated *Dll1* expression upon Notch disruption, suggesting rapid stem cell remodeling. Whether this response is key to maintaining CBCs until Paneth cells return or is, perhaps, a marker of impending CBC differentiation will be important future questions to pursue.

Crypt hyperproliferation and activation of multipotential progenitors are hallmarks of the intestinal regenerative response. The damage induced by Notch niche interruption is different from previously described crypt injury methods that induce CBC loss, including genetic, radiation, or chemotherapeutic drug treatment approaches. In our study, a robust regenerative response was observed although CBCs were retained. Our observations are in accordance with another study that observed modest increases in proliferation and crypt height after depletion of all secretory cells, including Paneth cells, from the adult mouse (Kim et al., 2012). Whether this response relates to Notch-signaling changes was not examined.

We observed that acute Notch inhibition activates *Dll1*+ cells to function as multipotential progenitors to generate all types of differentiated epithelial cells while CBC function is diminished. The generation of enterocytes from

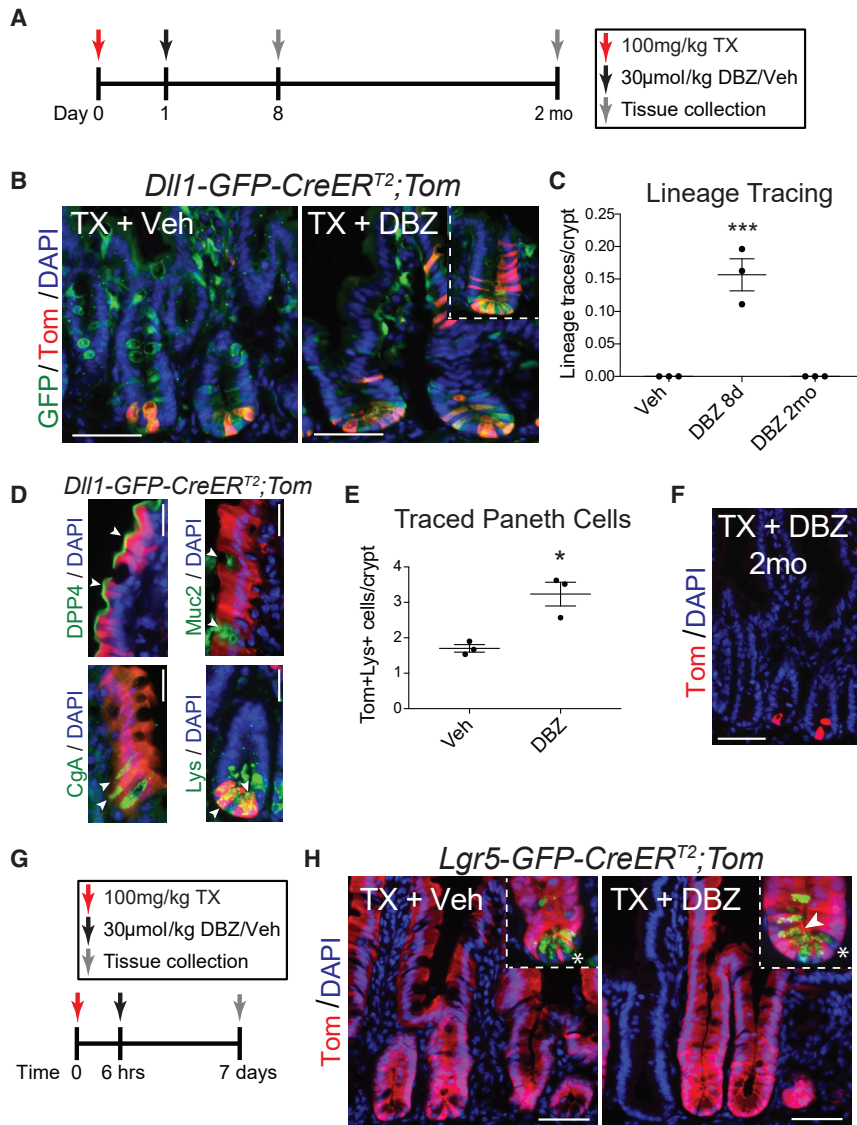


Figure 6. Multiple Progenitor Cell Populations Generate Paneth Cells after Notch Inhibition

(A) Analysis of lineage tracing from *Dll1*-expressing cells. Schematic of the experimental design using *Dll1-GFP-CreER^{T2};Tom* mice treated with TX, followed by Veh or DBZ, with duodenal tissue harvested at 8 days or 2 months post-TX, as indicated. (B and F) Intestinal tissue sections were stained for GFP (green) to visualize *Dll1*-expressing cells, and RFP (red) was visualized for Tom lineage-marked cells at day 8 (B) and 2 months (F). (B) The inset shows an example of a lineage trace. Scale bars, 50 μm.

(C) The number of lineage traces per crypt, defined as a ribbon of four or more Tom+ cells, were counted. Quantitative data are presented as mean ± SEM (**p = 0.0005 Veh versus DBZ by one-way ANOVA and Dunnett's post-test; n = 3 mice/group). Sixty to 120 crypts were counted per mouse. (D) Analysis of differentiated cells generated by *Dll1+* progenitors activated by DBZ treatment. Day 8 lineage tracing in *Dll1-GFP-CreER^{T2};Tom* mice co-staining for Tom (red) and markers (green) of enterocytes (DPP4), goblet cells (Muc2), endocrine cells (CgA), or Paneth cells (Lys), with DAPI (blue). Arrowheads mark examples of co-stained cells. Scale bars, 20 μm.

(E) Paneth cells arising from *Dll1+* progenitors were identified and quantified at day 8 by visualizing Tom/Lys double-positive cells. Quantitative data are presented as mean ± SEM (*p = 0.012 Veh versus DBZ by Student's t test; n = 3 mice/group). 60–120 crypts were counted per mouse.

(G and H) Analysis of lineage tracing from *Lgr5* CBC stem cells. (G) Schematic of the experimental design using *Lgr5-GFP-CreER^{T2};Tom* mice treated with TX followed by Veh or DBZ treatment, with duodenal tissue harvested at day 7 post-TX. (H) Tom lineage tracing (red) from *Lgr5* CBCs is displayed. Insets show Tom/Lys co-staining, demonstrating a subset of Tom-marked Paneth cells. Arrowhead, Tom/Lys co-stained cell; asterisk, Lys only stained cell. Scale bars, 50 μm.

See also Figure S5.

Dll1+ cells is unusual as these progenitors are normally restricted to secretory cell types (van Es et al., 2012). However, the activated *Dll1+* multipotential progenitors did not contribute to the CBC pool and thus did not function as FSCs. This contrasts with a previous study showing that *Dll1+* secretory progenitors can regenerate CBCs lost after crypt damage caused by radiation (van Es et al., 2012). Thus, our study suggests that the two FSC functions of activation to maintain the epithelium and regenerate lost CBCs can be disconnected. Importantly, we observed that CBCs also contribute to restoration of the depleted Paneth cell pool. Thus, multiple progenitor cell populations can

replenish these cells to repair the Notch niche. Our findings suggest that activation of epithelial cells to effect crypt repair is dependent on the specific cellular damage induced by the injury, underscoring the cellular plasticity and exquisite drive to regain homeostasis in the crypt.

To conclude, our studies highlight the exceptional cellular plasticity of the intestine and characterize the remodeling response to transient CBC niche inhibition. We propose a process whereby acute Notch inhibition stimulates a regenerative response stemming from rapid Paneth cell loss and impaired CBC activity, which is fueled in part by *Dll1+* cell expansion and activation. Our study

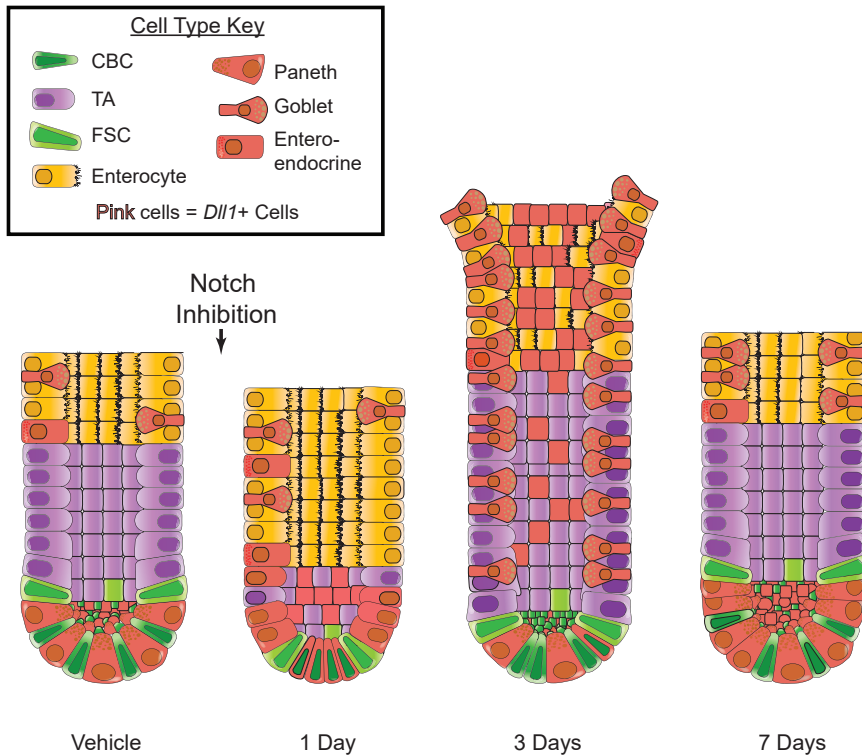


Figure 7. Crypt Cell Remodeling Following Acute Notch Inhibition

Schematic of the dynamic cellular changes in the intestinal crypt after transient Notch inhibition. Cells are color coded as indicated. One day after Notch inhibition, Paneth cells are lost by apoptosis, CBC function is impaired, *Dll1*+ cells increase, with *Dll1*-expression activated in CBCs. At day 3, a regenerative response is observed with increased proliferation associated with expansion of Notch ligand-expressing cells and enhanced Notch signaling. At this time, Paneth cells are returning to the crypt base and CBC function resumes. Multiple progenitors replenish the depleted Paneth cell pool, including *Dll1*+ progenitors and CBCs. By day 7 the crypt has largely returned to homeostasis. CBCs are maintained throughout the remodeling process despite their functional changes.

introduces acute Notch inhibition as a novel crypt disruption model which opens the door to studying mechanisms of CBC and Paneth cell responses during crypt repair.

EXPERIMENTAL PROCEDURES

Mice

Lgr5-GFP-CreER^{T2} (Jackson Lab 008875) (Barker et al., 2007), *Olfm4-GFP-CreER^{T2}* (from Hans Clevers) (Schuijers et al., 2014), *Defensin α 4-Cre* (Burger et al., 2018), *Dll1-mCherry* and *Dll4-mCherry* BAC transgenic mice (Chakrabarti et al., 2018; Tikhonova et al., 2019), *Dll1-GFP-CreER^{T2}* (from Hans Clevers) (van Es et al., 2012), *Hopx-CreER* (Jackson Laboratory, 017606) (Takeda et al., 2011), *ROSA26-LSL-tdTomato* (*Tom*; Jackson Laboratory, 007908) (Madisen et al., 2010), or *ROSA26-LSL-mTmG* (*mTmG*; Jackson Laboratory, 007576) (Muzumdar et al., 2007) alleles were verified by PCR genotyping. All mice were maintained on a C57BL/6 background, with the exception of *Defensin α 4-Cre;Tom* used for DLL1/DLL4 antibody inhibition experiments (Figure S1), which were on a mixed background. Mice were housed in ventilated and automated watering cages with a 12-h light cycle under specific pathogen-free conditions. Protocols for mouse usage were approved by the University of Michigan Committee on Use and Care of Animals. Adult mice of both sexes were used for analyses.

Animal Treatment Protocols and Tissue Collection

Mice were injected intraperitoneally with DBZ (30 μ mol/kg) (SYN-COM, Netherlands) or Veh as described (van Es et al., 2005), and intestinal tissue was collected at various timepoints. Some mice

were injected with EdU (25 mg/kg) (Life Technologies) 1.5 h before tissue collection. Intestinal tissue was fixed in 4% paraformaldehyde overnight for paraffin sections as described (VanDussen et al., 2012). Tissue prepared for frozen sections was fixed for 1 h and incubated in 30% sucrose overnight before embedding in OCT (Tissue-Tek). Some mice were treated with a single intraperitoneal injection of 100 mg/kg TX prior to DBZ or Veh treatment as described (Bohin et al., 2018). *Defensin α 4-Cre;Tom* mice were treated with a mixture of humanized neutralizing monoclonal antibodies directed against DLL1 and DLL4, or an irrelevant isotype control antibody against herpes simplex virus gD protein (Ridgway et al., 2006; Wu et al., 2010), injected intraperitoneally at 15 mg/kg each for two daily doses with intestinal tissue collected the next day.

Immunohistology

Paraffin sections (4–5 μ m) were stained with periodic acid-Schiff/Alcian blue (Newcomer Supply, cat. no. 9162B, 1003A) to visualize mucin-containing goblet cells. Immunostaining with rabbit anti-lysozyme (1:200, DAKO, cat. no. A0099), rabbit anti-GFP (1:200, Invitrogen, cat. no. A21311), rabbit anti-cleaved caspase-3 (1:50, Cell Signal, cat. no. 9664S), rabbit anti-Muc2 (1:200, Santa Cruz, cat. no. sc-15334), rabbit anti-chromogranin A (1:200, Abcam, cat. no. ab15160), and goat anti-DPP4 (1:200, Millipore, cat. no. SAB2500328) was performed as described (Lopez-Diaz et al., 2006). Co-staining for cleaved caspase-3 and MMP7 was performed by co-incubating rabbit anti-cleaved caspase-3 with rat anti-MMP7 (1:400, Vanderbilt, cat. no. 4,334). Rabbit anti-cleaved NOTCH1 (NICD; 1:50, Cell Signal, cat. no. 4147S) staining used



a TSA SuperBoost kit (Thermo, no. B40943). EdU-Click-iT kit (Life Technologies, cat. no. C10337) was used to identify proliferating cells. Images were captured on a Nikon E800 microscope with Olympus DP controller software.

In situ Hybridization

Olfm4 in situ hybridization was performed on paraffin sections as described (Carulli et al., 2015). *Lgr5* in situ hybridization was performed on frozen sections as described (Demitrack et al., 2015).

Quantitative Morphometric Analyses

Morphometric quantification of cellular proliferation (EdU+), crypt cellularity (DAPI+), Notch signaling (NICD+), apoptosis (cleaved caspase-3+), and lineage-traced Paneth cells (Tom+/Lys+) were measured by counting positive or co-positive cells per well-oriented crypt. Lineage tracing counted the number of Tom+ cells per crypt, defined as a ribbon of four or more Tom+ cells. The numbers of crypts counted are indicated in figure legends. Morphometric analyses were completed using ImageJ software (<http://imagej.nih.gov/ij/>).

Crypt Isolation and Gene Expression Analysis

Crypts were isolated from mouse duodenum as described (Carulli et al., 2015). RNA was isolated using RNeasy Mini kit with DNase I treatment as per manufacturer instructions (QIAGEN). cDNA was reverse transcribed with the iScript cDNA synthesis kit (Bio-Rad) using 1 µg of total RNA. qPCR was performed as described (Lopez-Diaz et al., 2006). *Olfm4*, *Lgr5*, *Notch1*, and *Notch2* primers were as described (Demitrack et al., 2015; Gifford et al., 2017; VanDusen et al., 2012). *Dll1* primers: CTG AGG TGT AAG ATG GAA GCG (forward); CAA CTG TCC ATA GTG CAA TGG (reverse). *Dll4* primers: TCG TCG TCA GGG ACA AGA ATA GC (forward); CTC GTC TGT TCG CCA AAT CTT ACC (reverse). mRNA abundance was normalized to *Hprt* with primers: AGG ACC TCT CGA AGT GTT GGA TAC (forward); AAC TTG CGC TCA TCT TAG GCT TTG (reverse).

FACS mCherry+ Cells to Form Organoids

A previously described protocol for isolation, plating and culturing *Lgr5*-GFP+ antral stem cells was adapted for the FACS isolation of single *Dll1*-mCherry+ duodenal crypt cells from Veh- and DBZ-treated mice, and their subsequent culture in Matrigel to form organoids (Demitrack et al., 2015). The efficiency of organoid formation was determined by counting organoids 7 days after plating and normalizing to the number of plated *Dll1*-mCherry+ cells (1,000 cells per well).

Statistical Analyses

Prism software (GraphPad) was used for statistical analysis. All statistical comparisons were performed with three to eight biological replicates per group. Quantitative data are presented as mean ± SEM. Comparisons were analyzed between two groups with unpaired two-tailed Student's t test and between three or more groups by one-way ANOVA with Dunnett's post-test. Significance is reported as *p < 0.05, **p < 0.01, ***p < 0.001, ****p < 0.0001.

SUPPLEMENTAL INFORMATION

Supplemental Information can be found online at <https://doi.org/10.1016/j.stemcr.2020.05.010>.

AUTHOR CONTRIBUTIONS

A.J.C. and L.C.S. initially conceived the project, with subsequent conceptual contributions from N.B. and T.M.K. Methodology was developed by T.M.K., N.B., A.J.C., E.M.W., and L.C.S. The majority of the investigation and analysis was carried out by T.M.K. and N.B., with contributions from A.J.C., E.M.W., E.A.C., J.C.J., C.D.B., and P.J.D. Resources were provided by C.W.S., J.G., I.A., M.W.R., and M.G.M. N.B. and L.C.S. wrote the manuscript and all authors provided critical feedback. L.C.S. provided supervision and obtained funding.

ACKNOWLEDGMENTS

We thank Y. Abushukur for technical help, E. Collin and L. Griffin for maintaining the mouse colonies, and E. Hibdon, K. McGowan, and N. Razumilava for critical comments on the manuscript. N.B. was supported by the Cellular and Molecular Biology Program, a Rackham research grant and the Benard L. Maas Fellowship. A.J.C. was supported by the Medical Scientist Training Program (T32-GM07863), the Center for Organogenesis (T32-HD007515), and a Ruth L Kirschstein NIH award (F30-DK095517). The research was funded by NIH R01-DK118023 to L.C.S., and Core support from the University of Michigan Gastrointestinal Research Center NIH P30-DK34933.

Received: August 4, 2019

Revised: May 12, 2020

Accepted: May 13, 2020

Published: June 11, 2020

REFERENCES

- Bankaitis, E.D., Ha, A., Kuo, C.J., and Magness, S.T. (2018). Reserve stem cells in intestinal homeostasis and injury. *Gastroenterology* 155, 1348–1361.
- Barker, N., van Es, J.H., Kuipers, J., Kujala, P., van den Born, M., Cozijnsen, M., Haegebarth, A., Korving, J., Begthel, H., Peters, P.J., et al. (2007). Identification of stem cells in small intestine and colon by marker gene *Lgr5*. *Nature* 449, 1003–1007.
- Bohin, N., Carlson, E.A., and Samuelson, L.C. (2018). Genome toxicity and impaired stem cell function after conditional activation of CreER(T2) in the intestine. *Stem Cell Reports* 11, 1337–1346.
- Burger, E., Araujo, A., Lopez-Yglesias, A., Rajala, M.W., Geng, L., Levine, B., Hooper, L.V., Burstein, E., and Yarovinsky, F. (2018). Loss of Paneth cell autophagy causes acute susceptibility to toxoplasma gondii-mediated inflammation. *Cell Host Microbe* 23, 177–190.
- Carulli, A.J., Keeley, T.M., Demitrack, E.S., Chung, J., Maillard, I., and Samuelson, L.C. (2015). Notch receptor regulation of intestinal stem cell homeostasis and crypt regeneration. *Dev. Biol.* 402, 98–108.



- Chakrabarti, R., Celia-Terrassa, T., Kumar, S., Hang, X., Wei, Y., Choudhury, A., Hwang, J., Peng, J., Nixon, B., Grady, J.J., et al. (2018). Notch ligand Dll1 mediates cross-talk between mammary stem cells and the macrophageal niche. *Science* 360. <https://doi.org/10.1126/science.aan4153>.
- Degirmenci, B., Valenta, T., Dimitrieva, S., Hausmann, G., and Basler, K. (2018). GLI1-expressing mesenchymal cells form the essential Wnt-secreting niche for colon stem cells. *Nature* 558, 449–453.
- Demitrack, E.S., Gifford, G.B., Keeley, T.M., Carulli, A.J., VanDussen, K.L., Thomas, D., Giordano, T.J., Liu, Z., Kopan, R., and Samuelson, L.C. (2015). Notch signaling regulates gastric antral LGR5 stem cell function. *EMBO J.* 34, 2522–2536.
- Dempsey, P.J., Bohin, N., and Samuelson, L.C. (2018). Notch pathway regulation of intestinal stem cell fate. In *Physiology of the Gastrointestinal Tract*, H.M. Said, F.K. Ghishan, J.D. Kaunitz, J.L. Merchant, and J.D. Wood, eds. (Elsevier/Academic Press), pp. 141–183.
- Durand, A., Donahue, B., Peignon, G., Letourneur, F., Cagnard, N., Slomianny, C., Perret, C., Shroyer, N.F., and Romagnolo, B. (2012). Functional intestinal stem cells after Paneth cell ablation induced by the loss of transcription factor Math1 (Atoh1). *Proc. Natl. Acad. Sci. U S A* 109, 8965–8970.
- Farin, H.F., Van Es, J.H., and Clevers, H. (2012). Redundant sources of Wnt regulate intestinal stem cells and promote formation of Paneth cells. *Gastroenterology* 143, 1518–1529.
- Fre, S., Huyghe, M., Mourikis, P., Robine, S., Louvard, D., and Artavanis-Tsakonas, S. (2005). Notch signals control the fate of immature progenitor cells in the intestine. *Nature* 435, 964–968.
- Garabedian, E.M., Roberts, L.J., McNevin, M.S., and Gordon, J.I. (1997). Examining the role of Paneth cells in the small intestine by lineage ablation in transgenic mice. *J. Biol. Chem.* 272, 23729–23740.
- Gifford, G.B., Demitrack, E.S., Keeley, T.M., Tam, A., La Cunza, N., Dedhia, P.H., Spence, J.R., Simeone, D.M., Saotome, I., Louvi, A., et al. (2017). Notch1 and Notch2 receptors regulate mouse and human gastric antral epithelial cell homeostasis. *Gut* 66, 1001–1011.
- Greicius, G., Kabiri, Z., Sigmundsson, K., Liang, C., Bunte, R., Singh, M.K., and Virshup, D.M. (2018). PDGFRalpha(+) pericyptal stromal cells are the critical source of Wnts and RSPO3 for murine intestinal stem cells in vivo. *Proc. Natl. Acad. Sci. U S A* 115, E3173–E3181.
- Ireland, H., Houghton, C., Howard, L., and Winton, D.J. (2005). Cellular inheritance of a Cre-activated reporter gene to determine Paneth cell longevity in the murine small intestine. *Dev. Dyn.* 233, 1332–1336.
- Jones, J.C., Brindley, C.D., Elder, N.H., Myers, M.G., Jr., Rajala, M.W., Dekaney, C.M., McNamee, E.N., Frey, M.R., Shroyer, N.F., and Dempsey, P.J. (2019). Cellular plasticity of Defa4(Cre)-expressing Paneth cells in response to notch activation and intestinal injury. *Cell Mol. Gastroenterol. Hepatol.* 7, 533–554.
- Kim, T.H., Escudero, S., and Shivdasani, R.A. (2012). Intact function of Lgr5 receptor-expressing intestinal stem cells in the absence of Paneth cells. *Proc. Natl. Acad. Sci. U S A* 109, 3932–3937.
- Lopez-Diaz, L., Hinkle, K.L., Jain, R.N., Zavros, Y., Brunkan, C.S., Keeley, T., Eaton, K.A., Merchant, J.L., Chew, C.S., and Samuelson, L.C. (2006). Parietal cell hyperstimulation and autoimmune gastritis in cholera toxin transgenic mice. *Am. J. Physiol. Gastrointest. Liver Physiol.* 290, G970–G979.
- Madisen, L., Zwingman, T.A., Sunkin, S.M., Oh, S.W., Zariwala, H.A., Gu, H., Ng, L.L., Palmiter, R.D., Hawrylycz, M.J., Jones, A.R., et al. (2010). A robust and high-throughput Cre reporting and characterization system for the whole mouse brain. *Nat. Neurosci.* 13, 133–140.
- Milano, J., McKay, J., Dagenais, C., Foster-Brown, L., Pognan, F., Gadiant, R., Jacobs, R.T., Zacco, A., Greenberg, B., and Ciaccio, P.J. (2004). Modulation of notch processing by gamma-secretase inhibitors causes intestinal goblet cell metaplasia and induction of genes known to specify gut secretory lineage differentiation. *Toxicol. Sci.* 82, 341–358.
- Montgomery, R.K., Carlone, D.L., Richmond, C.A., Farilla, L., Kraendonk, M.E., Henderson, D.E., Baffour-Awuah, N.Y., Ambruzs, D.M., Fogli, L.K., Algra, S., et al. (2011). Mouse telomerase reverse transcriptase (mTert) expression marks slowly cycling intestinal stem cells. *Proc. Natl. Acad. Sci. U S A* 108, 179–184.
- Muzumdar, M.D., Tasic, B., Miyamichi, K., Li, L., and Luo, L. (2007). A global double-fluorescent Cre reporter mouse. *Genesis* 45, 593–605.
- Pellegrinet, L., Rodilla, V., Liu, Z., Chen, S., Koch, U., Espinosa, L., Kaestner, K.H., Kopan, R., Lewis, J., and Radtke, F. (2011). Dll1- and dll4-mediated notch signaling are required for homeostasis of intestinal stem cells. *Gastroenterology* 140, 1230–1240.
- Powell, A.E., Wang, Y., Li, Y., Poulin, E.J., Means, A.L., Washington, M.K., Higginbotham, J.N., Juchheim, A., Prasad, N., Levy, S.E., et al. (2012). The pan-ErbB negative regulator Lrig1 is an intestinal stem cell marker that functions as a tumor suppressor. *Cell* 149, 146–158.
- Riccio, O., van Gijn, M.E., Bezdek, A.C., Pellegrinet, L., van Es, J.H., Zimmer-Strobl, U., Strobl, L.J., Honjo, T., Clevers, H., and Radtke, F. (2008). Loss of intestinal crypt progenitor cells owing to inactivation of both Notch1 and Notch2 is accompanied by derepression of CDK inhibitors p27Kip1 and p57Kip2. *EMBO Rep.* 9, 377–383.
- Ridgway, J., Zhang, G., Wu, Y., Stawicki, S., Liang, W.C., Chanthery, Y., Kowalski, J., Watts, R.J., Callahan, C., Kasman, I., et al. (2006). Inhibition of Dll4 signalling inhibits tumour growth by deregulating angiogenesis. *Nature* 444, 1083–1087.
- Rodriguez-Colman, M.J., Schewe, M., Meerlo, M., Stigter, E., Gerits, J., Pras-Raves, M., Sacchetti, A., Hornsveld, M., Oost, K.C., Snippert, H.J., et al. (2017). Interplay between metabolic identities in the intestinal crypt supports stem cell function. *Nature* 543, 424–427.
- Roth, S., Franken, P., Sacchetti, A., Kremer, A., Anderson, K., Sansom, O., and Fodde, R. (2012). Paneth cells in intestinal homeostasis and tissue injury. *PLoS One* 7, e38965.
- San Roman, A.K., Jayewickreme, C.D., Murtaugh, L.C., and Shivdasani, R.A. (2014). Wnt secretion from epithelial cells and subepithelial myofibroblasts is not required in the mouse intestinal stem cell niche in vivo. *Stem Cell Reports* 2, 127–134.



- Sangiorgi, E., and Capecchi, M.R. (2008). Bmi1 is expressed in vivo in intestinal stem cells. *Nat. Genet.* 40, 915–920.
- Santos, A.J.M., Lo, Y.H., Mah, A.T., and Kuo, C.J. (2018). The intestinal stem cell niche: homeostasis and adaptations. *Trends Cell Biol.* 28, 1062–1078.
- Sasaki, N., Sachs, N., Wiebrands, K., Ellenbroek, S.I., Fumagalli, A., Lyubimova, A., Begthel, H., van den Born, M., van Es, J.H., Karthaus, W.R., et al. (2016). Reg4+ deep crypt secretory cells function as epithelial niche for Lgr5+ stem cells in colon. *Proc. Natl. Acad. Sci. U S A* 113, E5399–E5407.
- Sato, T., van Es, J.H., Snippert, H.J., Stange, D.E., Vries, R.G., van den Born, M., Barker, N., Shroyer, N.F., van de Wetering, M., and Clevers, H. (2011). Paneth cells constitute the niche for Lgr5 stem cells in intestinal crypts. *Nature* 469, 415–418.
- Schuijers, J., van der Flier, L.G., van Es, J., and Clevers, H. (2014). Robust cre-mediated recombination in small intestinal stem cells utilizing the *olm4* locus. *Stem Cell Reports* 3, 234–241.
- Sei, Y., Feng, J., Samsel, L., White, A., Zhao, X., Yun, S., Citrin, D., McCoy, J.P., Sundaresan, S., Hayes, M.M., et al. (2018). Mature enteroendocrine cells contribute to basal and pathological stem cell dynamics in the small intestine. *Am. J. Physiol. Gastrointest. Liver Physiol.* 315, G495–G510.
- Shoshkes-Carmel, M., Wang, Y.J., Wangenstein, K.J., Toth, B., Kondo, A., Massasa, E.E., Itzkovitz, S., and Kaestner, K.H. (2018). Subepithelial telocytes are an important source of Wnts that supports intestinal crypts. *Nature* 557, 242–246.
- Stanger, B.Z., Datar, R., Murtaugh, L.C., and Melton, D.A. (2005). Direct regulation of intestinal fate by Notch. *Proc. Natl. Acad. Sci. U S A* 102, 12443–12448.
- Takeda, N., Jain, R., LeBoeuf, M.R., Wang, Q., Lu, M.M., and Epstein, J.A. (2011). Interconversion between intestinal stem cell populations in distinct niches. *Science* 334, 1420–1424.
- Tetteh, P.W., Basak, O., Farin, H.F., Wiebrands, K., Kretschmar, K., Begthel, H., van den Born, M., Korving, J., de Sauvage, F., van Es, J.H., et al. (2016). Replacement of lost Lgr5-positive stem cells through plasticity of their enterocyte-lineage daughters. *Cell Stem Cell* 18, 203–213.
- Tian, H., Biehs, B., Chiu, C., Siebel, C.W., Wu, Y., Costa, M., de Sauvage, F.J., and Klein, O.D. (2015). Opposing activities of Notch and Wnt signaling regulate intestinal stem cells and gut homeostasis. *Cell Rep.* 11, 33–42.
- Tian, H., Biehs, B., Warming, S., Leong, K.G., Rangell, L., Klein, O.D., and de Sauvage, F.J. (2011). A reserve stem cell population in small intestine renders Lgr5-positive cells dispensable. *Nature* 478, 255–259.
- Tikhonova, A.N., Dolgalev, I., Hu, H., Sivaraj, K.K., Hoxha, E., Cuesta-Dominguez, A., Pinho, S., Akhmetzyanova, I., Gao, J., Witkowski, M., et al. (2019). The bone marrow microenvironment at single-cell resolution. *Nature* 569, 222–228.
- Tsai, Y.H., VanDussen, K.L., Sawey, E.T., Wade, A.W., Kasper, C., Rakshit, S., Bhatt, R.G., Stoeck, A., Maillard, I., Crawford, H.C., et al. (2014). ADAM10 regulates Notch function in intestinal stem cells of mice. *Gastroenterology* 147, 822–834.
- van der Flier, L.G., van Gijn, M.E., Hatzis, P., Kujala, P., Haegebarth, A., Stange, D.E., Begthel, H., van den Born, M., Guryev, V., Oving, I., et al. (2009). Transcription factor achaete scute-like 2 controls intestinal stem cell fate. *Cell* 136, 903–912.
- van Es, J.H., Sato, T., van de Wetering, M., Lyubimova, A., Yee Nee, A.N., Gregorieff, A., Sasaki, N., Zeinstra, L., van den Born, M., Korving, J., et al. (2012). Dll1+ secretory progenitor cells revert to stem cells upon crypt damage. *Nat. Cell Biol.* 14, 1099–1104.
- van Es, J.H., van Gijn, M.E., Riccio, O., van den Born, M., Vooijs, M., Begthel, H., Cozijnsen, M., Robine, S., Winton, D.J., Radtke, F., et al. (2005). Notch/gamma-secretase inhibition turns proliferative cells in intestinal crypts and adenomas into goblet cells. *Nature* 435, 959–963.
- van Es, J.H., Wiebrands, K., Lopez-Iglesias, C., van de Wetering, M., Zeinstra, L., van den Born, M., Korving, J., Sasaki, N., Peters, P.J., van Oudenaarden, A., et al. (2019). Enteroendocrine and tuft cells support Lgr5 stem cells on Paneth cell depletion. *Proc. Natl. Acad. Sci. U S A* 116, 26599–26605.
- VanDussen, K.L., Carulli, A.J., Keeley, T.M., Patel, S.R., Puthoff, B.J., Magness, S.T., Tran, I.T., Maillard, I., Siebel, C., Kolterud, A., et al. (2012). Notch signaling modulates proliferation and differentiation of intestinal crypt base columnar stem cells. *Development* 139, 488–497.
- Wu, Y., Cain-Hom, C., Choy, L., Hagenbeek, T.J., de Leon, G.P., Chen, Y., Finkle, D., Venook, R., Wu, X., Ridgway, J., et al. (2010). Therapeutic antibody targeting of individual Notch receptors. *Nature* 464, 1052–1057.
- Yan, K.S., Chia, L.A., Li, X., Ootani, A., Su, J., Lee, J.Y., Su, N., Luo, Y., Heilshorn, S.C., Amieva, M.R., et al. (2012). The intestinal stem cell markers Bmi1 and Lgr5 identify two functionally distinct populations. *Proc. Natl. Acad. Sci. U S A* 109, 466–471.
- Yan, K.S., Janda, C.Y., Chang, J., Zheng, G.X.Y., Larkin, K.A., Luca, V.C., Chia, L.A., Mah, A.T., Han, A., Terry, J.M., et al. (2017). Non-equivalence of Wnt and R-spondin ligands during Lgr5(+) intestinal stem-cell self-renewal. *Nature* 545, 238–242.
- Yu, S., Tong, K., Zhao, Y., Balasubramanian, I., Yap, G.S., Ferraris, R.P., Bonder, E.M., Verzi, M.P., and Gao, N. (2018). Paneth cell multipotency induced by notch activation following injury. *Cell Stem Cell* 23, 46–59.